Few-Body Systems (EFB23) manuscript No.
(will be inserted by the editor)

Jonas Braun · **Hans-Werner Hammer**

Electric Properties of One-Neutron Halo Nuclei in Halo EFT

arXiv:1612.07689v1 [nucl-th] 22 Dec 2016

Received: date / Accepted: date

Abstract We exploit the separation of scales in weakly-bound nuclei to compute E2 transitions and electric form factors in a Halo EFT framework. The relevant degrees of freedom are the core and the halo neutron. The EFT expansion is carried out in powers of R_{core}/R_{halo}, where R_{core} and R_{halo} denote the length scales of the core and halo, respectively. We include the strong s-wave and d-wave interactions by introducing dimer fields. The dimer propagators are regulated by employing the power divergence subtraction scheme and matched to the effective range expansion in the respective channel. Electromagnetic interactions are included via minimal substitution in the Lagrangian. We demonstrate that, depending on the observable and respective partial wave, additional local gauge-invariant operators contribute in LO, NLO and higher orders.

∗ This work has been supported by Deutsche Forschungsgemeinschaft (SFB 1245).

Keywords Halo EFT · Two-body system · Electric properties

1 Introduction

Electric properties provide a unique window on the structure and dynamics of one-neutron halo nuclei. Two prominent examples of one-neutron halo nuclei are ^{11}Be and ^{15}C [11]. Due to their weakly-bound nature, the length scales R_{halo} of the halo and R_{core} of the core are separated. As a consequence, observables can be calculated using Halo EFT [5; 4] which exploits this separation of scales between R_{core} and R_{halo}. The Halo EFT formalism has been successfully used to study various reactions and properties of halo-like systems. Some examples include s-wave $\alpha\alpha$ resonance in ^{8}Be [10], universal properties of two-neutron halo nuclei [6; 7], radiative neutron/proton capture on ^{7}Li [14; 18] and on ^{7}Be [17] and the ground state of ^{19}C [1]. In this work, we follow the approach presented in Ref. [9], where electric properties of ^{11}Be are calculated using Halo EFT. The $\frac{1}{2}^+$ ground state of ^{11}Be is predominantly an s-wave bound state and the $\frac{1}{2}^-$ first excited state predominantly a p-wave bound state.

We apply the Halo EFT framework to ^{15}C, which has also a $\frac{1}{2}^+$ ground state. In contrast to ^{11}Be, the first excited $\frac{5}{2}^+$ state of ^{15}C is predominantly a d-wave bound state. We include the strong d-wave interaction by introducing a new dimer field and compute electric form factors and the E2 transition strength. In a similar way, electromagnetic form factors for the ground state of ^{15}C and the radiative neutron capture on ^{14}C to the $\frac{1}{2}^+$ ground state of ^{15}C are calculated in Refs. [8; 15], respectively.

J. Braun
Institut für Kernphysik, Technische Universität Darmstadt, 64289 Darmstadt, Germany
E-mail: braun@theorie.ikp.physik.tu-darmstadt.de

H.-W. Hammer
Institut für Kernphysik, Technische Universität Darmstadt, 64289 Darmstadt, Germany
ExtreMe Matter Institute EMMI, GSI Helmholtzzentrum für Schwerionenforschung GmbH, 64291 Darmstadt, Germany

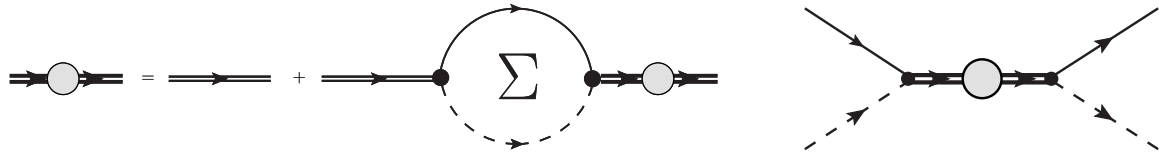

Fig. 1 The dashed line denotes the core field c, and the thin, solid line the neutron. The thin double line represents the bare dimer propagator, and the thick double line with the gray circle is the dressed dimer propagator. The left panel shows the diagrammatic representation of the Dyson equation for the dressed dimer propagator and the right panel the neutron-core scattering amplitude with the dressed dimer propagator.

2 Halo EFT formalism

The neutron separation energy of the $\frac{1}{2}^+$ state of ^{15}C is 1218 keV and the neutron separation energy of the $\frac{5}{2}^+$ state is 478 keV [2]. The first excitation of the ^{14}C nucleus is 6.1 MeV above the 0^+ ground state. Compared to the bound states of ^{14}C the weakly-bound states of ^{15}C indicate their one-neutron halo nature. Converting these energy scales into the relevant distance scales R_{core} and R_{halo} in this system we can carry out our EFT expansion in powers of $R_{core}/R_{halo} \approx 0.3-0.45$. Since the ratio is not particularly small, effects beyond LO are not negligible in our theory.

We follow the Halo EFT formalism developed in Ref. [9]. The relevant degrees of freedom are the ^{14}C core, represented by a bosonic field c, and the halo neutron, represented by a spinor field n. The strong s-wave and d-wave interactions are included through the incorporation of auxiliary spinor fields σ_s and d_m, which correspond to the $\frac{1}{2}^+$ and $\frac{5}{2}^+$ states, respectively. With the convention that repeated spin indices are summed, the non-relativistic Lagrangian is written as:

$$\begin{aligned}\mathscr{L} = {} & c^\dagger\left(i\partial_t + \frac{\nabla^2}{2M}\right)c + n^\dagger\left(i\partial_t + \frac{\nabla^2}{2m}\right)n \\ & + \sigma_s^\dagger\left[\eta_0\left(i\partial_t + \frac{\nabla^2}{2M_{nc}}\right) + \Delta_0\right]\sigma_s + d_m^\dagger\left[c_2\left(i\partial_t + \frac{\nabla^2}{2M_{nc}}\right)^2 + \eta_2\left(i\partial_t + \frac{\nabla^2}{2M_{nc}}\right) + \Delta_2\right]d_m \\ & - g_0\left[c^\dagger n_s^\dagger\sigma_s + \sigma_s^\dagger n_s c\right] - g_2\left[d_m^\dagger\left[n\overleftrightarrow{\nabla}^2 c\right]_{\frac{5}{2},m} + \left[c^\dagger\overleftrightarrow{\nabla}^2 n^\dagger\right]_{\frac{5}{2},m} d_m\right] , \end{aligned} \tag{1}$$

where $\overleftrightarrow{\nabla}$ is the Galilean invariant derivative, m denotes the neutron mass, M the core mass and $M_{nc} = m+M$ is the total mass of the n-^{14}C system and we project out the $J = 5/2$ part of the strong d-wave interaction.

2.1 Dressing the d-wave state

The dressed d propagator and the d-wave scattering amplitude are computed from the diagrams in Fig. 1 in the same way as in Ref. [9]. The Dyson equation for the d-wave is illustrated in the left panel of Fig. 1 with the one-loop self-energy $\Sigma_d(p)$. We use the power divergence subtraction (PDS) as regularization scheme [12; 13]. The d-wave scattering amplitude in the two-body center-of-mass frame with $E = k^2/(2m_R)$ and $k = |\mathbf{p}'| = |\mathbf{p}|$ for on-shell scattering is matched to the effective range expansion (ERE). Since we have to renormalize arising divergences, the effective range parameters a_2, r_2 and $\mathscr{P}_2$ are required at LO, which leads to the power-counting scheme below. Furthermore, we need the additional higher order kinetic term with coupling constant c_2 for the bare propagator in our Lagrangian (1) [3].

The assumed power counting for the $D_p(p)$ propagator follows the ideas of Refs. [4; 9; 15]. We apply the constraint to have the minimal number of fine tunings possible in our power-counting scheme. This requirement is motivated by the fact that every additional fine tuning makes our scenario less likely to be found in nature, as discussed in Ref. [4]. However, the number of fine tunings for higher partial waves ($l > 1$) is larger than proposed in Ref. [4]. Since arising divergences in the calculation of the dimer propagator have to be renormalized properly, the number of ERE parameters needed at LO for the l-th partial wave is $(l+1)$. Thus, for the l-th partial wave and $l \geq 1$ we need l fine-tuned parameters. This suggests that higher partial wave bound states are less likely to appear in nature which is consistent with experimental observations. In the case

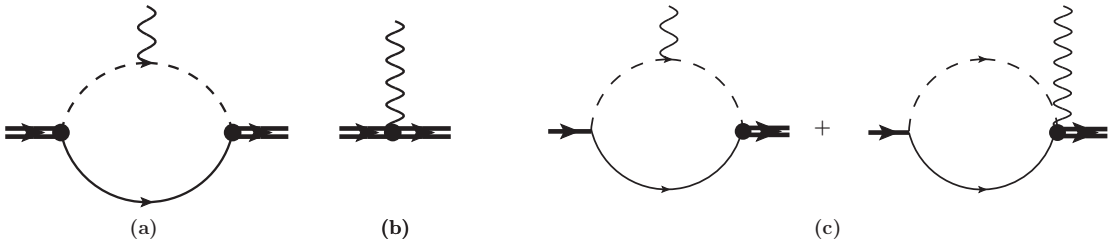

Fig. 2 The diagrams (a) and (b) contributing to the irreducible vertex for an A_0 photon to couple to the ^{14}C-neutron d-wave bound state field up to NLO. Diagram (a) emerges from the minimal substitution in the strong d-wave interaction and contributes at NLO while diagram (b) arises since r_2, $\mathscr{P}_2$ and the local, gauge-invariant operator $\sim L^{(d)}_{\text{C01}/2}$ contribute at LO. Diagram (c): The two LO diagrams contributing to the irreducible vertex that determines the s-to-d state transition in Halo EFT.

of the $D_d(p)$ propagator, two out of three ERE parameters need to be fine-tuned, because $a_2 \sim R^4_{halo}\, R_{core}$ and $r_2 \sim 1/(R^2_{halo}\, R_{core})$ are both unnaturally large. This scenario is more likely to occur than three unnaturally large parameters and three fine-tunings such that $\mathscr{P}_2 \sim 1/R_{core}$. Higher ERE terms are suppressed by powers of R_{core}/R_{halo}. Thus, the relevant fit parameters in our EFT at LO are γ_0, γ_2, r_2, and $\mathscr{P}_2$.

2.2 Electromagnetic interactions

Electromagnetic interactions are included via minimal substitution in the Lagrangian, $\partial_\mu \to D_\mu = \partial_\mu + ie\hat{Q}A_\mu$. Additionally, we have to consider further, local, gauge-invariant operators involving the electric field $\mathbf{E}$ and the fields c, n, σ and d. Depending on the observable and respective partial wave they contribute at different orders in our EFT.

3 Results

3.1 Electric form factors

The result for the electric form factor of the s-wave bound state is given in Ref. [9] for ^{11}Be and in Ref. [8] for ^{15}C. We follow the approach of the first reference and compute the d-wave form factors by calculating the contribution to the irreducible vertex for $A_0 dd$ interactions up to NLO shown in Fig. 2. The computation is carried out in the Breit frame, where $q = (0, \mathbf{q})$, and the irreducible vertex for the A_0 photon coupling to the d state in Cartesian coordinates yields:

$$\left\langle ij \left| J^0 \right| op \right\rangle = -ieQ_c \left[G_E(|\mathbf{q}|)\, E_{ij,op} + \frac{1}{2M^2_{nc}} G_Q(|\mathbf{q}|)\, Q_{ij,op} + \frac{1}{4M^4_{nc}} G_H(|\mathbf{q}|)\, H_{ij,op} \right] , \tag{2}$$

with the three momentum of the virtual photon $\mathbf{q} = \mathbf{p}' - \mathbf{p}$ and three different d-wave tensors for each form factor $E_{ij,op} \sim q^0$, $Q_{ij,op} \sim q^2$ and $H_{ij,op} \sim q^4$. The neutron spin is unaffected by the charge operator up to the order considered here and we get results for the electric $G_E(|\mathbf{q}|)$, quadrupole $G_Q(|\mathbf{q}|)$ and hexadecupole $G_H(|\mathbf{q}|)$ form factors. The local, gauge-invariant operator $\sim L^{(d)}_{\text{C01}/2}$ is needed at LO to counter the arising divergences for the charge radius and quadrupole moment. At LO we obtain the following results for the charge and quadrupole radii and the quadrupole and hexadecupole moment:

$$\langle r^2_E \rangle^{(d)} = \frac{-6\tilde{L}^{(d)\,\text{LO}}_{\text{C0}E}}{r_2 + \mathscr{P}_2\gamma_2^2}, \quad \langle r^2_Q \rangle^{(d)} = \frac{90 f^4}{7\gamma_2\left(r_2 + \mathscr{P}_2\gamma_2^2\right)}, \quad \mu^{(d)}_Q = \frac{40\tilde{L}^{(d)\,\text{LO}}_{\text{C02}}}{3\left(r_2 + \mathscr{P}_2\gamma_2^2\right)}, \quad \mu^{(d)}_H = \frac{-2f^4}{3\gamma_2\left(r_2 + \mathscr{P}_2\gamma_2^2\right)}, \tag{3}$$

with $f = m_R/M$. Since the quadrupole radius $\langle r^2_Q \rangle^{(d)}$ and the hexadecupole moment $\mu^{(d)}_H$ differ only by a constant factor at LO, we obtain a smooth correlation between both observables $\langle r^2_Q \rangle^{(d)} = -\frac{135}{7}\mu^{(d)}_H$.

3.2 E2 transition

The diagrams contributing to the irreducible vertex for the E2 transition from the $1/2^+$ state to the $5/2^+$ state at LO are shown in Fig. 2. The photon has a four momentum of $k = (\omega, \mathbf{k})$ and its polarization is denoted by μ. The computation of both diagrams yields a vertex function $\Gamma_{m's\mu}$, where m' is the total angular momentum projection of the $5/2^+$ state and s denotes the spin projection of the $1/2^+$ state. We calculate the irreducible vertex in Coulomb gauge such that we have $\mathbf{k}\cdot\boldsymbol{\varepsilon} = 0$ for real photons and obtain for B(E2):

$$\mathrm{B(E2)} = \frac{6}{15\pi}\, Z_{eff}^2 e^2\, \frac{\gamma_0}{-r_2 - \mathscr{P}_2\gamma_2^2} \left[\frac{3\gamma_0^2 + 9\gamma_0\gamma_2 + 8\gamma_2^2}{(\gamma_0+\gamma_2)^3}\right]^2 ,$$

where the effective charge is given by $Z_{eff} = \left(\frac{m}{M_{nc}}\right)^2 Q_c$ [16].

The experimental result for the E2 transition strength is $\mathrm{B(E2)_{W.u.}} = 0.44(1)$ and thus, $\mathrm{B(E2)} = 0.97(2)\ e^2\mathrm{fm}^4$. It follows that $1/\left(r_2 + \mathscr{P}_2\gamma_2^2\right) = -323(7)\ \mathrm{fm}^3$ and considering the previous section we can predict $\mu_H^{(d)} = 0.030\ e\mathrm{fm}^4$, $\langle r_Q^2\rangle^{(d)} = -0.578\ \mathrm{fm}^4$, and $\langle r_H^2\rangle^{(d)} = 0.004\ \mathrm{fm}^6$.

In the future, we plan to investigate the correlations found in Halo EFT in *ab initio* calculations.

References

1. Acharya B, Phillips DR (2013) 19 c in halo eft: Effective-range parameters from coulomb dissociation experiments. Nuclear Physics A 913:103–115
2. Ajzenberg-Selove F (1991) Energy levels of light nuclei a= 13–15. Nuclear Physics A 523(1):1–196
3. Beane SR, Savage MJ (2001) Rearranging pionless effective field theory. Nuclear Physics A 694(3):511–524
4. Bedaque PF, Hammer HW, Van Kolck U (2003) Narrow resonances in effective field theory. Physics Letters B 569(3):159–167
5. Bertulani C, Hammer HW, Van Kolck U (2002) Effective field theory for halo nuclei: shallow p-wave states. Nuclear Physics A 712(1):37–58
6. Canham DL, Hammer HW (2008) Universal properties and structure of halo nuclei. The European Physical Journal A 37(3):367–380
7. Canham DL, Hammer HW (2010) Range corrections for two-neutron halo nuclei in effective theory. Nuclear Physics A 836(3):275–292
8. Fernando L, Vaghani A, Rupak G (2015) Electromagnetic form factors of one neutron halos with spin 1/2+ ground state. arXiv preprint arXiv:151104054
9. Hammer HW, Phillips DR (2011) Electric properties of the beryllium-11 system in halo eft. Nuclear Physics A 865(1):17–42
10. Higa R, Hammer HW, van Kolck U (2008) $\alpha\alpha$ scattering in halo effective field theory. Nuclear Physics A 809(3):171–188
11. Jensen A, Riisager K, Fedorov DV, Garrido E (2004) Structure and reactions of quantum halos. Reviews of modern physics 76(1):215
12. Kaplan DB, Savage MJ, Wise MB (1998) A new expansion for nucleon-nucleon interactions. Physics Letters B 424(3):390–396
13. Kaplan DB, Savage MJ, Wise MB (1998) Two-nucleon systems from effective field theory. Nuclear Physics B 534(1):329–355
14. Rupak G, Higa R (2011) Model-independent calculation of radiative neutron capture on lithium-7. Physical review letters 106(22):222,501
15. Rupak G, Fernando L, Vaghani A (2012) Radiative neutron capture on carbon-14 in effective field theory. Physical Review C 86(4):044,608
16. Typel S, Baur G (2005) Electromagnetic strength of neutron and proton single-particle halo nuclei. Nuclear Physics A 759(3):247–308
17. Zhang X, Nollett KM, Phillips D (2014) Combining ab initio calculations and low-energy effective field theory for halo nuclear systems: The case of $^7\mathrm{Be} + n \to {}^8\mathrm{B} + \gamma$. Physical Review C 89(5):051,602
18. Zhang X, Nollett KM, Phillips DR (2014) Combining ab initio calculations and low-energy effective field theory for halo nuclear systems: The case of $^7\mathrm{Li} + n \to {}^8\mathrm{Li} + \gamma$. Physical Review C 89(2):024,613